

Axomorphic Perspective Projection Model for Immersive Imagery

Jakub Maksymilian Fober
jakub.m.fober@protonmail.com
talk@maxfober.space

Abstract

A wide choice of cinematic lenses enables motion-picture creators to adapt image visual-appearance to their creative vision. Such choice does not exist in the realm of real-time computer graphics, where only one type of perspective projection is widely used, a linear perspective. This paper presents an extended perspective imaging model, which can represent distortion and FoV parameters of entire variety of film and photographic lenses (e.g., wide-angle, fisheye, anamorphic), while preserving parametrization in an artistically convincing manner. Self-experimentation with the model revealed that each projection type provides accurate perception of a different aspect of depicted space (e.g., speed, distance, shape). Presented model, enables combination of multiple projections, each on a different axis of the image, to achieve optimal perception for a given scenario. This new projection, named *axomorphic*, was made available here, under an open license (CC BY-SA 3.0), for a wide and easy adoption.

CCS Concepts: • Computing methodologies → Perception; Ray tracing; • Human-centered computing; • Applied computing → Media arts;

Keywords: Curvilinear Perspective, Panini, Anamorphic, Cylindrical, Fisheye, lens Map

© 2021-2024 Jakub Maksymilian Fober



This work is licensed under Creative Commons BY-SA 3.0 license.
<https://creativecommons.org/licenses/by-sa/3.0/legalcode>
For all other options including custom licensing, contact the owner/author(s).

1 Introduction

The perspective in the computer real-time graphics hasn't changed since the dawn of CGI. It is based on a concept as old as the fifteenth-century Renaissance, a linear projection [Alberti 1435; Argan and Robb 1946; McArdle 2013]. This situation is similar to the beginnings of photography, where only one type of lens was widely used, an Anno Domini 1866 *Rapid Rectilinear* [Kingslake 1989] lens. Linear perspective even at the time of its advent, 500 years ago, has been criticized for distorting proportions [Da Vinci 1632]. In a phenomenon known today as *Leonardo's paradox* [Dixon 1987], in which figures further away but at the periphery

appear larger, than those located near the optical center. Computer graphics really skipped the artistic achievements of the last five centuries in regard to perspective. This includes the cylindrical perspective of Pannini [Sharpless et al. 2010], Barker [Wikipedia, contributors 2019], and anamorphic lenses used in cinematography [Giardina 2016; Neil 2004; Sasaki 2017a,b]. The situation is even more critical, as there is no mathematical model for generating anamorphic projection in an artistically-convincing manner [Yuan and Sasian 2009]. Some attempts were made at alternative projections for computer graphics, with fixed cylindrical or spherical geometry [Baldwin et al. 2014; Sharpless et al. 2010]. A parametrized perspective model was also proposed as a new standard [Correia and Romão 2007], but wasn't adopted. It included interpolation states in between rectilinear/equidistant and spherical/cylindrical projection. The cylindrical parametrization of this solution was merely an interpolation factor, where intermediate values did not correspond to any common projection type. Therefore, it was not well-suited for artistic or professional use.

1.1 Break from Axiom of Pyramid Frustum

The notion of sphere as a projective surface that incorporates cartographic mapping to produce a perspective picture became popularized [German et al. 2007; Peñaranda et al. 2015; Williams 2015]. Also, perspective parametrization that transitions according to the content (by the view-tilt angle) has been developed, as a modification to the computer game MINECRAFT [Williams 2017]. But the results of these solutions were more a gimmick and have not found practical use. The linear perspective projection was still the way-to-go for most digital content. Some state-of-the-art video games incorporated limited lens distortion, like RESIDENT EVIL series (after 2017), *Alan Wake 2* and more strongly *Unrecord*.

One of the reasons for a limited adoption of a non-linear projection was the fixed-function architecture of GPUs in regard to rasterization. But with the advent of real-time ray-tracing and variable shading-rate, more exotic projections could become widely adopted and integrated into the tools.

1.2 Presented New Model

This paper aims to provide a perspective model with a mathematical parametrization that allows artistic-style interaction with image geometry. Similar in a way film directors choose lenses for each scene based on aesthetics [Giardina

2016; Neil 2004; Sasaki 2017a], but with parametrization that offers a greater degree of control. It also provides a psycho-physiological correlation between perspective model parameters and the perception of depicted space attributes, like distance, size, proportions, shape or speed. That mapping enables the use of the presented model in a professional environment, where image geometry is specifically suited for a task [Whittaker 1984].

The presented perspective model is named *axomorphic* (from Greek *axon-*, axis + *morphē*, shape; “varying shape across axes”).

1.3 Document Naming Convention

This document uses the following naming convention:

- A left-handed coordinate system is used.
- Vectors are presented in column format.
- Matrices use row-major order and are denoted as “ $M_{\text{row col}}$ ”.
- Matrix multiplication is denoted as “[column] $_a$ · [row] $_b$ = M_{ab} ”.
- A single bar enclosure “ $|u|$ ” represents the absolute value of a scalar.
- A single bar enclosure “ $|\vec{v}|$ ” represents the length of a vector.
- Vectors with an arithmetic sign, or without, are calculated component-wise to form another vector.
- Centered dot “ \cdot ” represents the dot product of two vectors.
- Square brackets with a comma “[f, c]” denotes an interval.
- Square brackets with blanks “[$x \ y$]” denotes a vector or a matrix.
- The power of “ -1 ” implies the reciprocal of the value.
- The QED symbol “ \square ” marks the final result or output.

This naming convention simplifies the process of translating formulas into shader code.

2 Axomorphic Primary-ray Map

If we assume that a projective visual space is spherical [Fleck 1994; McArdle 2013], one can define perspective picture as an array of rays pointing to the surface of visual sphere. This is how the algorithm described below will output a viewing-ray map (aka lens map). Lens map is a two-dimensional \mathbb{R}^3 vector field representing viewing rays, where each ray is assigned to a screen pixel. Visual sphere as the image model enables wider angle of view, beyond the limit for planar projection of 180°. Such vector field can be easily converted to a cube UV map, ST map, or other screen distortion format.

Here, the procedural algorithm for lens map uses two types of input values from the user; distortion parameter for two principal axes and *focal-length* or *angle-of-view* (aka FoV). Two distinct principal axes define the axomorphic projection type. Each axis distortion profile is expressed by the

azimuthal projection factor k [Bettonvil 2005; Fleck 1994; Krause 2019]. Both principal axes share the same focal-length value f . The evaluation of each principal-axis distortion profile produces spherical angles $\vec{\theta}_x$ and $\vec{\theta}_y$. These angles are then combined to form the axomorphic azimuthal-projection angle θ' . The interpolation of $\vec{\theta}$ components is achieved through axomorphic weights $\vec{\varphi}_x$ and $\vec{\varphi}_y$, which are derived from the spherical angle φ of the azimuthal projection.

Note. Calculation of φ angle is omitted here, as view-coordinate \vec{v} alone allows for direct calculation of $\vec{\varphi}$ weights.

$$r = |\vec{v}| = \sqrt{\vec{v}_x^2 + \vec{v}_y^2} \quad (1a)$$

$$\vec{\theta}_x = \begin{cases} \frac{\arctan\left(\frac{r}{f} \vec{k}_x\right)}{\vec{k}_x}, & \text{if } \vec{k}_x > 0 \\ \frac{r}{f}, & \text{if } \vec{k}_x = 0 \\ \frac{\arcsin\left(\frac{r}{f} \vec{k}_x\right)}{\vec{k}_x}, & \text{if } \vec{k}_x < 0 \end{cases} \quad (1b)$$

$$\vec{\theta}_y = \begin{cases} \frac{\arctan\left(\frac{r}{f} \vec{k}_y\right)}{\vec{k}_y}, & \text{if } \vec{k}_y > 0 \\ \frac{r}{f}, & \text{if } \vec{k}_y = 0 \\ \frac{\arcsin\left(\frac{r}{f} \vec{k}_y\right)}{\vec{k}_y}, & \text{if } \vec{k}_y < 0 \end{cases} \quad (1c)$$

$$\begin{bmatrix} \vec{\varphi}_x \\ \vec{\varphi}_y \end{bmatrix} = \begin{bmatrix} \cos^2 \varphi \\ \sin^2 \varphi \end{bmatrix} = \begin{bmatrix} \frac{1}{2} + \frac{\cos(2\varphi)}{2} \\ \frac{1}{2} - \frac{\cos(2\varphi)}{2} \end{bmatrix} = \begin{bmatrix} \frac{\vec{v}_x^2}{\vec{v}_x^2 + \vec{v}_y^2} \\ \frac{\vec{v}_y^2}{\vec{v}_x^2 + \vec{v}_y^2} \end{bmatrix}, \quad (1d)$$

where $r \in \mathbb{R}_{>0}$ is the view-coordinate radius (vector magnitude). Vector $\vec{\theta} \in [0, \pi]^2$ contains incidence angles (measured from the optical axis) of two azimuthal projections. Vector $\vec{\varphi} \in [0, 1]^2$ contains the axomorphic interpolation weights, which are linear $\vec{\varphi}_x + \vec{\varphi}_y = 1$, but exhibit spherical distribution (see Figure 1 on the facing page). Vector $\vec{k} \in [-1, 1]^2$ (also $[-1, 1]^3$ in a variant from subsection 2.2) describes two power axes of axomorphic projection. The algorithm is evaluated per-pixel for position $\vec{v} \in \mathbb{R}^2$ in view-space coordinates, centered at the optical axis and normalized at the chosen angle-of-view (horizontal or vertical). The final axomorphic incidence angle θ' is obtained through interpolation of $\vec{\theta}$ components by $\vec{\varphi}$ weights.

$$\theta' = \begin{bmatrix} \vec{\theta}_x \\ \vec{\theta}_y \end{bmatrix} \cdot \begin{bmatrix} \vec{\varphi}_x \\ \vec{\varphi}_y \end{bmatrix} = \vec{\theta}_x \vec{\varphi}_x + \vec{\theta}_y \vec{\varphi}_y \quad (2a)$$

$$\begin{bmatrix} \hat{G}_x \\ \hat{G}_y \\ \hat{G}_z \end{bmatrix} = \begin{bmatrix} \sin \theta' \cos \varphi \\ \sin \theta' \sin \varphi \\ \cos \theta' \end{bmatrix} = \begin{bmatrix} \frac{\sin \theta'}{r} \vec{v}_x \\ \frac{\sin \theta'}{r} \vec{v}_y \\ \cos \theta' \end{bmatrix}, \quad \square \quad (2b)$$

here $\theta' \in (0, \pi]$ is the axomorphic incidence angle, measured from the optical axis. This measurement resembles azimuthal projection of a globe (here a visual sphere) [McArdle 2013]. The final incidence vector $\hat{G} \in [-1, 1]^3$ (aka viewing-ray) is obtained from the axomorphic angle θ' . Parameters $r, \vec{v}, \vec{\varphi}$

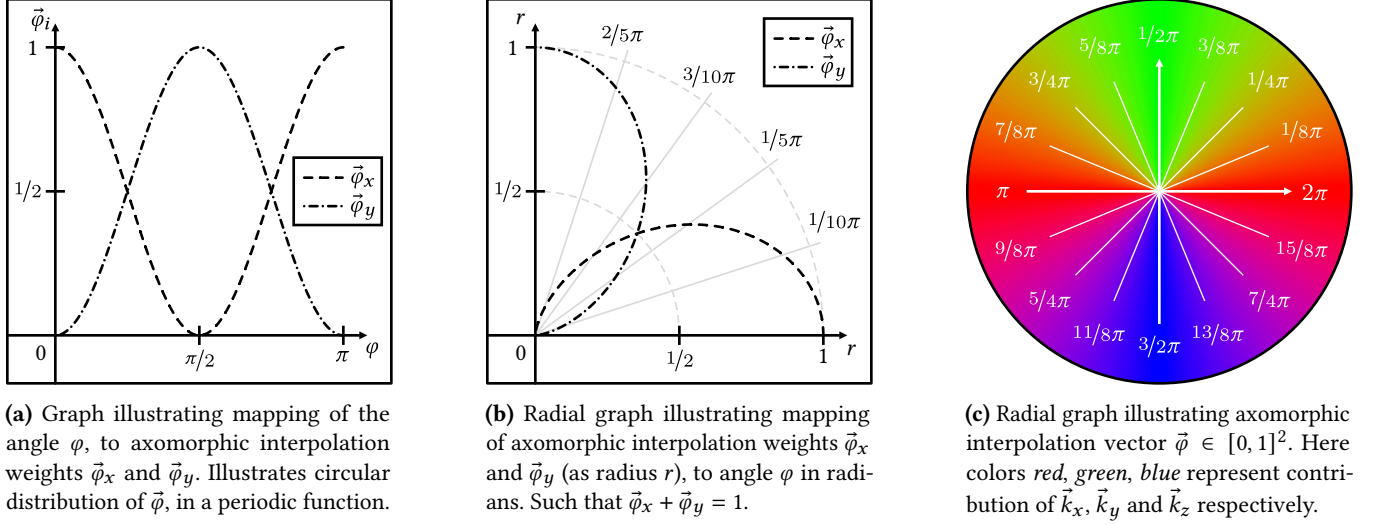


Figure 1. Illustrating correlation between the axomorphic interpolation weights $\vec{\varphi}_x$, $\vec{\varphi}_y$ and the spherical angle φ .

are in view-space, while $\vec{\theta}$, θ' , φ , \hat{G} are in visual-sphere space. Essentially, the axomorphic primary-ray map preserves the azimuthal angle φ while modulating only the radius of the image.

Inverse Mapping. It can be obtained through a lookup mesh shaped as a tessellated screen-plane, mapped to the visual-sphere surface by equation (2). This mesh can be directly sampled by a ray to read the UV coordinates, or rasterized to a UV coordinates map. Ray-mesh sampling offers the advantage of an unlimited angle-of-view compared to texture sampling, which is practically limited to around $140^\circ\Omega$.

2.1 Focal Length and Angle-of-View

To enhance control over the image, a mapping between the angle-of-view Ω and the focal length f can be established. Here, the focal length is expressed in reciprocal format to optimize its use in equation (1).

$$f^{-1} = \begin{cases} \frac{\tan\left(\frac{\Omega_h}{2} \vec{k}_x\right)}{r \vec{k}_x}, & \text{if } \vec{k}_x > 0 \\ \frac{\Omega_h}{2r}, & \text{if } \vec{k}_x = 0 \\ \frac{\sin\left(\frac{\Omega_h}{2} \vec{k}_x\right)}{r \vec{k}_x}, & \text{if } \vec{k}_x < 0, \end{cases} \quad (3)$$

where $\Omega_h \in (0, \tau]$ denotes horizontal angle of view, and r denotes radius at Ω . Similarly, vertical Ω_v can be obtained using \vec{k}_y parameter instead. The resultant value $1/f \in \mathbb{R}_{>0}$ is the reciprocal focal-length.

Remark. The focal-length f value must be the same for both $\vec{\theta}_x$ and $\vec{\theta}_y$. Therefore, only one reference angle Ω can be chosen, either horizontal or vertical.

Inverse function, to equation (3), for angle-of-view Ω , from focal-length f , is obtained as follows:

$$\Omega_v = \begin{cases} 2 \frac{\arctan\left(\frac{r \vec{k}_y}{f}\right)}{\vec{k}_y}, & \text{if } \vec{k}_y > 0 \\ 2 \frac{r}{f}, & \text{if } \vec{k}_y = 0 \\ 2 \frac{\arcsin\left(\frac{r \vec{k}_y}{f}\right)}{\vec{k}_y}, & \text{if } \vec{k}_y < 0, \end{cases} \quad (4)$$

This formula can be used to obtain the actual vertical angle-of-view from a horizontally established focal length. Similarly horizontal angle Ω_h can be obtained using the \vec{k}_x parameter. Here input value r denotes radius at Ω .

2.2 Asymmetrical Axomorphism

Parameter \vec{k}_y can be further augmented to produce an asymmetrical axomorphic projection by introducing a third input value denoted as \vec{k}_z . In such a case, the bottom and top halves of the image can present different azimuthal projections along the axis.

$$\vec{k}'_y = \begin{cases} \vec{k}_z, & \text{if } \vec{v}_y < 0 \\ \vec{k}_y, & \text{otherwise,} \end{cases} \quad (5)$$

therefore \vec{k}'_y replaces \vec{k}_y in equations (1), (4) and (6).

Asymmetrical axomorphism can be applied to any side of the principal axes. A use case for such a perspective could be in racing, where the bottom half of the screen contains an image of the road. Choosing equidistant projection (which preserves angular speed) would provide an accurate perception of velocity. The top half of the screen contains the image of opponent vehicles or the road ahead. Choosing stereographic projection (which preserves angles and proportions) would provide an enhanced perception for choosing the optimal trajectory. For the horizontal power axis, choosing

Value of k	Azimuthal projection type
$k_i = 1$	Rectilinear (Gnomonic)
$k_i = 1/2$	Stereographic
$k_i = 0$	Equidistant
$k_i = -1/2$	Equisolid
$k_i = -1$	Orthographic (azimuthal)

Source: PTGui 11 fisheye factor [Krause 2019].

(a) Primary k values and corresponding azimuthal projection type.

Azimuthal projection type	Perception of space
Rectilinear	straight lines
Stereographic	shapes, angles
Equidistant	speed, aim position
Equisolid	distances, sizes
Orthographic (azimuthal)	brightness (no vignetting)

Source: Properties of azimuthal projections and empirical self study using various video games with shader overlay, by ReShade shader injection.

(b) Azimuthal projection type and corresponding enhancement for a given space attribute perception.

Table 1. Tables presenting perspective parameters, corresponding projection type and associated perception attitude.

equisolid projection (which preserves distance) would enhance the perception of distance to the turn for braking.

2.3 Vignetting Mask

Vignetting is a crucial visual symbol indicating the stretching of the visual sphere by the projection. Incorporating a vignetting effect with a custom projection enhances spatial perception.

Here, the vignetting mask is obtained in the same way for all axomorphic, anamorphic, and spherical projections. It is generated as the ratio of the circumference of a small circle ($2\pi \sin \theta'$) to the circumference of the image circle ($2\pi r_i$), where the image circle's radius r_i is obtained through the normalization of the picture-space radius r by the focal length f .

$$\Lambda = \begin{cases} 1, & \text{if } r = 0 \\ \frac{\sin \theta'}{r} f, & \text{else, } \square \end{cases} \quad (6)$$

where $\Lambda \in [0, 1]$ is the axomorphic vignetting mask value, which is inversely proportional to the scaling of visual sphere surface in image space.

Note. In the shader implementation, conditional branching can be omitted as equation $\frac{\sin \theta'}{0}$ will automatically yield 1.

This vignetting model accounts for the natural falloff due to the stretching of the projected visual sphere. In real optical systems, the vignetting effect is often enhanced at the borders by the gradual occlusion of the aperture, especially at lower f-stops. At lower f-stops, some lens casing elements can block the entrance pupil at steep angles, usually when the aperture is wide-open. Therefore presented model is closest achieved at lowest apertures, when the entrance pupil is small and vignetting is closest to natural.

3 Converting Ray-map to ST-map

The ray/lens-map can be easily converted to the ST-map format for distorting a rectilinear source image, provided that the maximum view angle Ω does not exceed or equal 180° .

Picture content type	Axomorphic \vec{k} values
Racing	$\vec{k} = \begin{bmatrix} -1/2 & 1/2 & 0 & \end{bmatrix}$
Flying	$\vec{k} = \begin{bmatrix} 1/2 & 0 & -1/2 & \end{bmatrix}$
First-person (generic)	$\vec{k} = \begin{bmatrix} 1/2 & 22/25 & 22/25 & \end{bmatrix}$
First-person (aiming)	$\vec{k} = \begin{bmatrix} 0 & 1/2 & 1/2 & \end{bmatrix}$
Pan motion	$\vec{k}_x \neq \vec{k}_y$
Roll motion	$\vec{k}_y = \vec{k}_x$
Tilt motion ^a	$\vec{k}_y \rightarrow \vec{k}_x$

Source: Values determined empirically with self experimentation using various competitive video games, in accordance to data in Table 1b.

^aMapping of vertical distortion by a tilt motion introduced first in a Minecraft mod [Williams 2017].

Table 2. Recommended values of \vec{k} , for various scenario and parameter behavior for a given camera motion type.

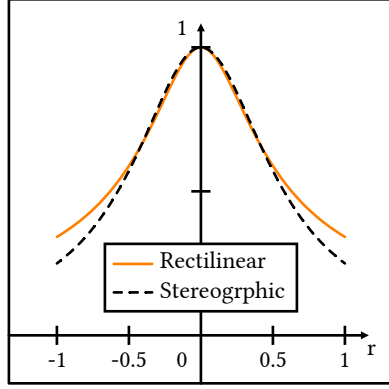
$$\begin{bmatrix} \vec{a}_x & \vec{a}_y \end{bmatrix} = \begin{cases} \begin{bmatrix} 1 & \frac{w}{h} \end{bmatrix}, & \text{if } \Omega_h \\ \begin{bmatrix} \frac{h}{w} & 1 \end{bmatrix}, & \text{if } \Omega_v \end{cases} \quad (7a)$$

$$\begin{bmatrix} \vec{f}_s \\ \vec{f}_t \end{bmatrix} = \frac{\cot \frac{\Omega}{2}}{2\hat{G}_z} \begin{bmatrix} \hat{G}_x \\ \hat{G}_y \end{bmatrix} \begin{bmatrix} \vec{a}_x \\ \vec{a}_y \end{bmatrix} + \frac{1}{2}, \quad \square \quad (7b)$$

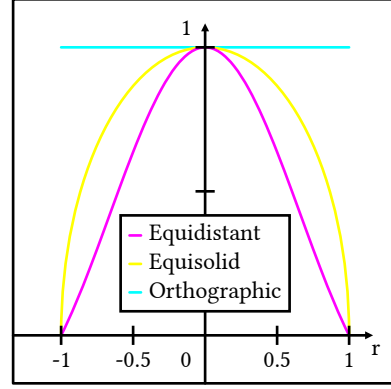
where $\vec{a} \in \mathbb{R}^2$ is the square-mapping vector for both the horizontal and vertical angle of view. Values w and h represent picture width and height, respectively. $\Omega < \pi$ is the angle of view. $\vec{f} \in [0, 1]^2$ represent the final ST-map vector. $\hat{G} \in [0, 1]^3$ is the input viewing-ray map vector.

4 Axomorphic Lens Distortion

The presented perspective model can be used to mimic the real-world anamorphic lens and its effects. Effects such as *disproportionate lens breathing* using focal length-based parametrization, which are unique to anamorphic photography [Neil 2004; Sasaki 2017b]. Some additional lens-corrections may



(a) Image radius to vignetting intensity graph, for Rectilinear projection at $140^\circ\Omega$ and for Stereographic projection at $240^\circ\Omega$.



(b) Image radius to vignetting intensity graph, for Equidistant and Equisolid projection at $360^\circ\Omega$ and for Orthographic (azimuthal) projection at $180^\circ\Omega$.

Figure 2. Plotting of vignetting intensity across the image radius, for each azimuthal projection at various Ω angles.

be added to the initial ray-map, to simulate more complex lens distortions and lens imperfections.

Below, an algorithm for axomorphic distortion of view coordinates is presented, which can be used as an input for viewing-ray map algorithm (equation 1 on page 2). The algorithm is based on the BROWN-CONRADY lens-distortion model [Wang et al. 2008] in a division variant [Fitzgibbon 2001]. It is executed on a view-coordinate \vec{v} , forming alternative vector \vec{v}' .

$$\begin{bmatrix} \vec{f}_x \\ \vec{f}_y \end{bmatrix} = \underbrace{\begin{bmatrix} \vec{v}_x - \vec{c}_1 \\ \vec{v}_y - \vec{c}_2 \end{bmatrix}}_{\text{cardinal offset } a} \quad (8a)$$

$$\begin{bmatrix} \vec{\phi}_x \\ \vec{\phi}_y \end{bmatrix} = \begin{bmatrix} \frac{\vec{f}_x^2}{\vec{f}_x^2 + \vec{f}_y^2} & \frac{\vec{f}_y^2}{\vec{f}_x^2 + \vec{f}_y^2} \end{bmatrix}^T \quad (8b)$$

$$r^2 = \vec{f}_x^2 + \vec{f}_y^2 \quad (8c)$$

$$\begin{bmatrix} \vec{v}'_x \\ \vec{v}'_y \end{bmatrix} = \begin{bmatrix} \vec{f}_x \\ \vec{f}_y \end{bmatrix} \underbrace{\left(\begin{bmatrix} 1 + \vec{k}_{x1}r^2 + \vec{k}_{x2}r^4 \dots \\ 1 + \vec{k}_{y1}r^2 + \vec{k}_{y2}r^4 \dots \end{bmatrix} \cdot \begin{bmatrix} \vec{\phi}_x \\ \vec{\phi}_y \end{bmatrix} \right)^{-1}}_{\text{radial axomorphic}} \quad \square \quad (8d)$$

$$\begin{bmatrix} \vec{f}_x \\ \vec{f}_y \end{bmatrix} \underbrace{\left(\begin{bmatrix} \vec{f}_x \\ \vec{f}_y \end{bmatrix} \cdot \begin{bmatrix} \vec{p}_1 \\ \vec{p}_2 \end{bmatrix} \right)}_{\text{decentering}} + r^2 \underbrace{\begin{bmatrix} \vec{q}_1 \\ \vec{q}_2 \end{bmatrix}}_{\text{thin prism}} + \underbrace{\begin{bmatrix} \vec{c}_1 \\ \vec{c}_2 \end{bmatrix}}_{\text{cardinal } b} \quad \square$$

$$\begin{bmatrix} \vec{v}'_x \\ \vec{v}'_y \end{bmatrix} \mapsto \begin{bmatrix} \hat{G}_x \\ \hat{G}_y \\ \hat{G}_z \end{bmatrix}, \quad \square \quad (8e)$$

where \vec{c}_1, \vec{c}_2 are the cardinal-offset parameters, \vec{q}_1, \vec{q}_2 are the thin-prism distortion parameters and \vec{p}_1, \vec{p}_2 are the decentering parameters. A set of \vec{k} parameters define radial distortion for each axomorphic power axis. \vec{v} is the input view-coordinate, and \vec{v}' is the view coordinate with applied lens-transformation. $\vec{\phi} \in [0, 1]^2$ is the axomorphic interpolation weight, defined in section 2 on page 2.

5 Axomorphic Chromatic Aberration

A chromatic aberration effect can be achieved with multi-sample blur, where each sample layer is colored with the corresponding spectral-value [Gilcher 2015]. Presented periodic function for spectral color $\vec{\chi}$ produces samples that always add up to 1 (neutral white) when number of samples is even. It also exhibits the correct order of spectrum colors.

$$\begin{bmatrix} \vec{\chi}_r \\ \vec{\chi}_g \\ \vec{\chi}_b \end{bmatrix} = \begin{matrix} 1 \\ 0 \end{matrix} \text{clamp} \left(\frac{3}{2} - \left| 4 \bmod \left(t + \begin{bmatrix} 1/4 \\ 0 \\ 3/4 \end{bmatrix}, 1 \right) - 2 \right| \right), \quad (9)$$

where $\vec{\chi} \in [0, 1]^3$ is the spectral-color value for position $t \in [0, 1]$ (see figure 4 on page 7 for more information).

Performing a spectral blur on an image involves the sum of multiple spectrum-colored layers. Scalar t (here replaced by sample progress) should never reach 1, which ensures preservation of picture's white-balance. The number of samples n must be an even number, and no less than 2 for a correct, neutral-white result.

$$\begin{bmatrix} \vec{f}'_r \\ \vec{f}'_g \\ \vec{f}'_b \end{bmatrix} = \frac{2}{n} \sum_{i=0}^{n-1} \begin{bmatrix} \vec{f}_r \\ \vec{f}_g \\ \vec{f}_b \end{bmatrix} \underbrace{\begin{matrix} 1 \\ 0 \end{matrix} \text{clamp} \left(\frac{3}{2} - \left| 4 \bmod \left(\frac{i}{n} + \begin{bmatrix} 1/4 \\ 0 \\ 3/4 \end{bmatrix}, 1 \right) - 2 \right| \right)}_{\vec{\chi} \text{ periodic function}}, \quad (10)$$

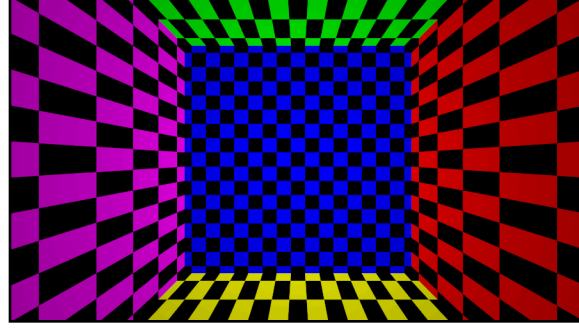
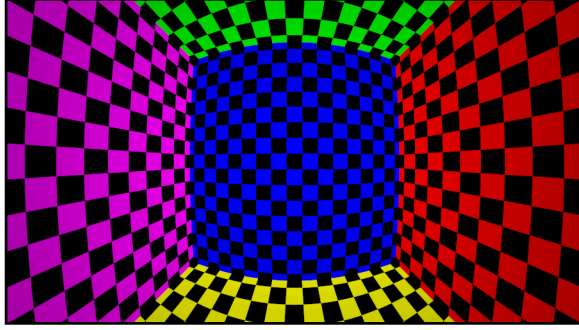
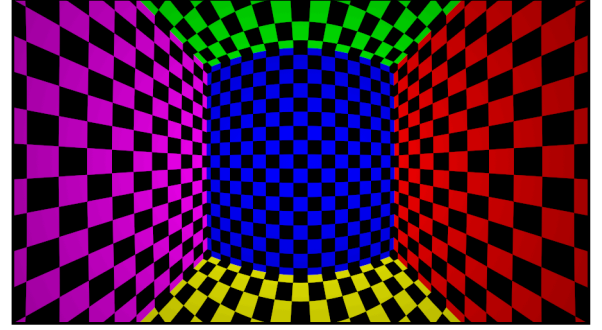
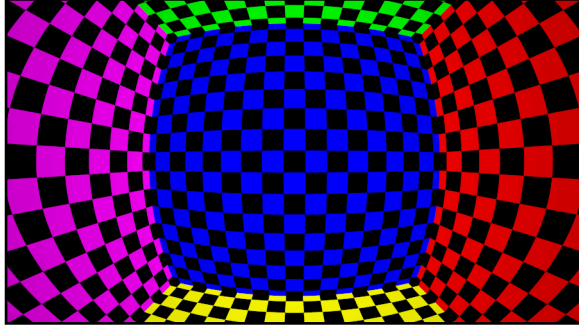
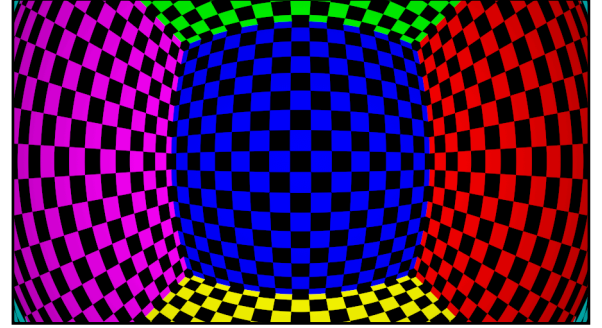
(a) $k = 1$, Rectilinear (standard).(b) $\vec{k} = [1/2 \quad 22/25]$, first-person (anamorphic style).(c) $\vec{k} = [1/2 \quad 1]$, panini.(d) $\vec{k} = [1/2 \quad 0 \quad -1/2]$, flying (asymmetrical).(e) $\vec{k} = [-1/2 \quad 1/2 \quad 0]$, racing (asymmetrical).

Figure 3. Example of various wide-angle ($\Omega_v \approx 110^\circ$) axomorphic-azimuthal projections with vignetting in $4/3^2$ aspect-ratio. The checkerboard depicts a cube centered at the observation point, with each face colored according to the axis direction. Here, primary colors represent the positive axis, and neighboring complementary colors its negative equivalent (same as in the color-wheel), $\{Mg, Yl, Cy\} \leftrightarrow -\{X, Y, Z\} \mapsto \{R, G, B\}$.

where $n \in 2\mathbb{N}_1$ is the even number of samples for the chromatic aberration color-split. $\vec{f} \in [0, 1]^3$ is the current-sample position color-value. $\vec{f}' \in [0, 1]^3$ is the final spectral-blurred color value.

The equation for spectral color $\vec{\chi}$ can be rewritten to a more optimized form, for parallel computation.

$$\begin{bmatrix} \vec{\chi}_r \\ \vec{\chi}_g \\ \vec{\chi}_b \end{bmatrix} = \begin{bmatrix} \text{clamp}_0^1(3/2 - |4t - 1|) \\ \text{clamp}_0^1(3/2 - |4t - 2|) \\ -\text{clamp}_0^1(3/2 - |4t - 1|) \end{bmatrix} + \begin{bmatrix} \text{clamp}_0^1(4t - 7/2) \\ 0 \\ 1 - \text{clamp}_0^1(4t - 7/2) \end{bmatrix}, \quad (11)$$

where $\vec{\chi} \in [0, 1]^3$ is the spectral color at position $t \in [0, 1]$. See the figure 4 on the facing page for visualization.

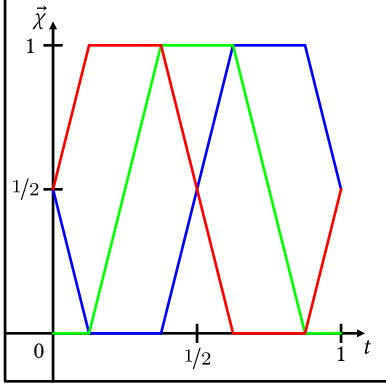


Figure 4. Mapping of $t \in [0, 1]$ to spectral color $\vec{\chi} \in [0, 1]^3$, for emulation of chromatic aberration. This is an output of periodic function, found in equation (9). Distribution of the values ensures proper color order and sum-of-samples with guaranteed neutral-white tint.

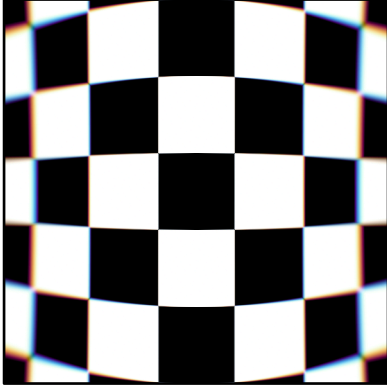


Figure 5. Example of axomorphic lens distortion with chromatic aberration, where $\vec{k}_{x1} = -0.25$, $\vec{k}_{y1} = 0.04$, $d = 0.5$, with 64-spectral samples.

5.1 Chromatic Aberration through Lens Distortion

Chromatic aberration can be integrated into lens distortion with spectral blurring, through the lens-transformation vector $\Delta\vec{v}$. Below, the equation for the spectral-blur displacement vector \vec{s} is presented, calculated per sample at position t .

$$\begin{bmatrix} \Delta\vec{v}_x \\ \Delta\vec{v}_y \end{bmatrix} = \begin{bmatrix} \vec{v}'_x - \vec{v}_x \\ \vec{v}'_y - \vec{v}_y \end{bmatrix} \quad (12a)$$

$$\begin{bmatrix} \vec{s}_x \\ \vec{s}_y \end{bmatrix} = \left(1 + \left(t - \frac{1}{2}\right)d\right) \begin{bmatrix} \Delta\vec{v}_x \\ \Delta\vec{v}_y \end{bmatrix}, \quad (12b)$$

where $\vec{s} \in \mathbb{R}^2$ is the spectral blur sample-offset vector at position $t \in [0, 1)$. Value $d \in \mathbb{R}$ denotes the lens dispersion-scale. For a visually pleasing result, additional blur pass can be applied, which direction is perpendicular to the \vec{s} vector,

and smaller in magnitude, as below.

$$\begin{bmatrix} \vec{s}'_x \\ \vec{s}'_y \end{bmatrix} = \frac{1}{4} \begin{bmatrix} -\vec{s}_y \\ \vec{s}_x \end{bmatrix}, \quad (13)$$

where \vec{s}' is the second-pass blur direction vector.

Figure 5 presents the final effect of two-pass blur, where the first pass is spectral, along lens-distortion $\Delta\vec{v}$, and the second-pass (of quarter-magnitude) is perpendicular $\perp \Delta\vec{v}$. A combination of both adds a defocusing effect to the image distortion.

6 Final Thoughts

In this paper, a mathematical model for generating various asymmetrical axomorphic perspective projections has been provided, along with perception-driven distortion-design recommendations. In the model, each principal axis of the image resembles some azimuthal projection exactly, while regions in-between are transitional, creating a hybrid projection. This way, advantage can be taken of many projection types, to create an optimal, tailored view for a given specific scenario. Such perception-driven parametrization enables the picture's geometry to adapt to the context, allowing dynamic adjustments on-the-fly in an artistically convincing manner.

In addition to axomorphic perspective, this paper presents vignetting effects and lens distortion with integrated chromatic aberration. The selection of these key features, enables almost complete digital lens simulation, for an immersive-imagery production.

Additional shader implementation of this technique can be found in the open-source `PerfectPerspective.fx` shader available on GitHub or via ReShade platform.

6.1 Prospects for Future Improvement

In the future, wide choice of cinematic lenses may be totally replaced by a post-production technique or an in-camera special effect, performed on-stage. Such technical solution would require several new technologies, like perhaps universal camera system, consisting of:

- Universal lens:
 - With parallax aberration correction and carefully mapped distortion.
- Universal camera sensor:
 - In correlation with the lens would produce distortion-free picture.
- Universal perspective algorithm:
 - Satisfied with this document.

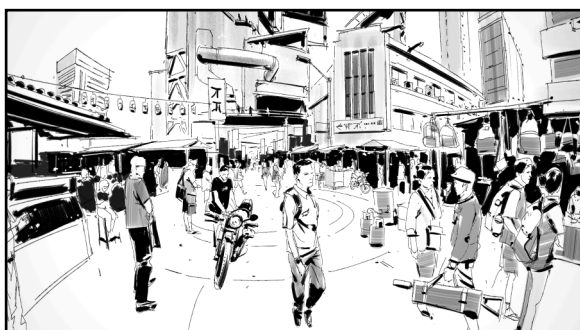
Acknowledgments

I would like to thank Anna and Stanley Sobczynski for their help, putting finishing touches on this document.



Panorama source: Captured from FOR HONOR through Nvidia Ansel.

(a) $\vec{k} = [1/2 \ 1]$, $f = 0.6$, $\Omega_h \approx 159^\circ$, panini preset, which along vertical axis, preserves straight lines, and along horizontal axis preserves proportions.



Panorama source: "China town" by JAMA JURABAEV.

(c) $\vec{k} = [0 \ 1 \ 4/5]$, $\Omega_h = 180^\circ$, artistic projection where background architecture points straight-up. Attention is focused at the center figure by compression of periphery, and proper composition is achieved by expansion of the bottom field.



Panorama source: Captured from WAR THUNDER through Nvidia Ansel.

(b) $\vec{k} = [1/2 \ 0 \ -1/2]$, $f = 0.6$, $\Omega_h \approx 159^\circ$, flying (asymmetrical), where bottom-half preserves distance, horizon preserves shape, and top-half preserves speed.



Panorama source: "The Lighthouse" by VLADIMIR SOMOV.

(d) $\vec{k} = [1/2 \ 0 \ 5/8]$, $\Omega_h = 195^\circ$, artistic projection with wide vertical field and limited bottom field, preserving proportion on the horizontal axis.

Figure 6. Examples of super wide-angle views in axomorphic projection with natural vignetting. Mapped from various 360° panoramas in equirectangular projection.

References

- Leon B. Alberti. 1435. *On Painting* (1970 ed.). New Haven: Yale University Press. <http://www.noteaccess.com/Texts/Alberti/index.htm>
- Giulio C. Argan and Nesca A. Robb. 1946. The Architecture of Brunelleschi and the Origins of Perspective Theory in the Fifteenth Century. *Journal of the Warburg and Courtauld Institutes* 9 (1946), 96. <https://doi.org/10.2307/750311>
- Joseph Baldwin, Alistair Burleigh, and Robert Pepperell. 2014. Comparing Artistic and Geometrical Perspective Depictions of Space in the Visual Field. *i-Perception* 5, 6 (jan 2014), 536–547. <https://doi.org/10.1068/i0668>
- Felix Bettonvil. 2005. Fisheye lenses. *WGN, Journal of the International Meteor Organization* 33, 1 (2005), 11–12. https://ui.adsabs.harvard.edu/link_gateway/2005JIMO...33...9B/ADS_PDF
- José Correia and Luís Romão. 2007. Extended perspective system. In *Proceedings of the 25th eCAADe International Conference*. 185–192.
- Leonardo Da Vinci. 1632. *A treatise on painting* (2014 ed.). Project Gutenberg, Chapter Linear Perspective, 49–59. <http://gutenberg.org/ebooks/46915>
- Robert A. Dixon. 1987. *Mathographics*. Basil Blackell Limited, Chapter Perspective Drawings, 82–83.
- Andrew W. Fitzgibbon. 2001. Simultaneous linear estimation of multiple view geometry and lens distortion. In *Proceedings of the 2001 IEEE Computer Society Conference on Computer Vision and Pattern Recognition. CVPR 2001*, Vol. 1. IEEE Comput. Soc, Kauai, HI, USA. <https://doi.org/10.1109/cvpr.2001.990465>
- Margaret M. Fleck. 1994. *Perspective Projection: the Wrong Imaging Model*. techreport 95-01. Computer Science, University of Iowa. <https://mfleck.cs.illinois.edu/my-papers/stereographic-TR.pdf>
- Daniel M. German, Pablo D'Angelo, Michael Gross, and Bruno Postle. 2007. New Methods to Project Panoramas for Practical and Aesthetic Purposes. In *Computational Aesthetics in Graphics, Visualization, and Imaging*. The Eurographics Association. <https://doi.org/10.2312/COMPAESTH/COMPAESTH07/015-022>
- Carolyn Giardina. 2016. How 'The Hateful Eight' Cinematographer Revived Lenses From the 1960s. *The Hollywood Reporter* (Jan. 2016). <https://hollywoodreporter.com/news/how-hateful-eight-cinematographer-revived-852586> Online.
- Pascal Gilcher. 2015. YACA (Yet Another Chromatic Aberration). ReShade forum. <https://reshade.me/forum/shader-presentation/1133-yaca-yet-another-chromatic-aberration#8861> Forum post.

- Rudolf Kingslake. 1989. *A History of the Photographic Lens*. Academic Press, Chapter IV, 59–62.
- Erik Krause. 2019. *Fisheye Projection*. PanoTools wiki. https://wiki.panotools.org/index.php?title=Fisheye_Projection&oldid=16077 Online.
- James M. McArdle. 2013. From the corner of your eye?... Personal blog. <https://drjamesmcardle.com/2013/04/07/from-the-corner-of-your-eye/> Online.
- Iain A. Neil. 2004. Lenses in Cinematography. *Optics and Photonics News* 15, 1 (2004), 26. <https://doi.org/10.1364/opn.15.1.000026>
- Luis Peñaranda, Luiz Velho, and Leonardo Sacht. 2015. Real-time correction of panoramic images using hyperbolic Möbius transformations. *Journal of Real-Time Image Processing* 15, 4 (may 2015), 725–738. <https://doi.org/10.1007/s11554-015-0502-x>
- Dan Sasaki. 2017a. The Aesthetics of Anamorphic in Film and Digital. Panavision Inc. <https://vimeo.com/167052303> Video.
- Dan Sasaki. 2017b. The Five Pillars of Anamorphic - Disproportionate Breathing. Panavision Inc. <https://vimeo.com/167045643> Video.
- Thomas K. Sharpless, Bruno Postle, and Daniel M. German. 2010. Panini: A New Projection for Rendering Wide Angle Perspective Images. *Computational Aesthetics in Graphics Visualization, and Imaging* (2010). <https://doi.org/10.2312/COMPAESTH/COMPAESTH10/009-016>
- Jianhua Wang, Fanhuai Shi, Jing Zhang, and Yuncai Liu. 2008. A new calibration model of camera lens distortion. *Pattern Recognition* 41, 2 (2008), 607–615. <https://doi.org/10.1016/j.patcog.2007.06.012>
- Eric J. W. Whittaker. 1984. *The Stereographic Projection* (2001 ed.). University College Cardiff Press. <http://oldwww.iucr.org/iucr-top/comm/cteach/pamphlets/11/11.pdf>
- Wikipedia, contributors. 2019. Robert Barker (painter). *Wikipedia, The Free Encyclopedia* (2019). [http://en.wikipedia.org/w/index.php?title=Robert_Barker_\(painter\)&oldid=907715733#Biography](http://en.wikipedia.org/w/index.php?title=Robert_Barker_(painter)&oldid=907715733#Biography)
- Shaun E. Williams. 2015. Blinky. GitHub, Inc. <https://github.com/shaunlebron/blinky> Modification, Quake.
- Shaun E. Williams. 2017. Flex FOV. GitHub, Inc. <https://github.com/shaunlebron/flex-fov> Modification, Minecraft.
- Sheng Yuan and Jose Sasian. 2009. Aberrations of anamorphic optical systems I: the first-order foundation and method for deriving the anamorphic primary aberration coefficients. *Applied Optics* 48, 13 (2009), 2574. <https://doi.org/10.1364/ao.48.002574>

Received February 2021; revised August 2021; revised December 2023